Research Article

Existence of subsurface structures from aeromagnetic data interpretation of the crustal architecture around Ibi, Middle Benue, Nigeria

Naheem Banji Salawu[1] · Muyiwa Michael Orosun[2] · Leke Sunday Adebiyi[3] · Toyin Yusuf Abdulraheem[1] · Silas Sunday Dada[4]

Received: 19 August 2019 / Accepted: 10 February 2020 / Published online: 17 February 2020

Abstract
Aeromagnetic data acquired over Ibi area within the Middle Benue Trough, Nigeria, has been interpreted to successfully mapped regional structural features that are favorable for economic mineral deposits. The 3D Euler deconvolution technique provided estimated depth values for the regional structural features while the deduced source parameter imaging gave depth estimates to magnetic basement of the study area. The latter map shows two major sub-basins with depth values between 2700 m and 3300 m. Since the magnetic basement depth estimates could be used as a proxy for the thickness of sedimentary formation of the region, the sedimentary formation is sufficiently thick for fossil maturation and therefore confirms that hydrocarbon exploration may be plausible within the region. The combined assessment of magnetic source edge location and magnetic basement depth values offers valuable information on the subsurface configuration, which is very important for mineral and hydrocarbon exploration within Ibi area.

Keywords Aeromagnetic data · 3D Euler deconvolution · Upward continuation · 3D Analytic signal · Reduction-to-pole · Source parameter imaging

1 Introduction

The magnetic method is widely used for mapping important targets in mineral and hydrocarbon exploration projects [1–3], and data can be acquired in the air, on the ocean, from the ground, and in borehole, for a wide range of geological purposes [4]. Modern aeromagnetic survey is capable of mapping valuable geologic structures on a regional scale including concealed terrains due to the sophistication of modern technology to provide high-quality data [5–7].

The interpretation of aeromagnetic anomaly data for improved sources depth estimates and locations of structural features such as faults, folds and contacts requires the use of relevant standard techniques and good geological interpretation. The 3D analytic signal introduced by Nabighian [8] and further developed by Roset et al. [9] is one of the standard techniques used for the locations of structural features from aeromagnetic anomaly data. Other established techniques for source depth estimates include 3D Euler deconvolution [10, 11] and source parameter imaging [12].

In this study, we applied enhancement filters such as upward continuation and 3D analytic signal to map structural features. The 3D Euler deconvolution technique was used to estimate depth to the mapped structural features, while the source parameter imaging was used to estimate depths of magnetic basement. This approach is to unravel

✉ Naheem Banji Salawu, salawubanji@yahoo.com | [1]BS Geophysical and Consultancy Ltd., Ilorin, Nigeria. [2]Department of Physics, University of Ilorin, Ilorin, Nigeria. [3]Department of Physical Sciences, Landmark University, Omu-Aran, Nigeria. [4]Department of Geology and Mineral Sciences, Al-Hikmah University, Ilorin, Nigeria.

SN Applied Sciences (2020) 2:427 | https://doi.org/10.1007/s42452-020-2230-5

subsurface geologic information which is essential for mineral and hydrocarbon exploration projects within Ibi area of Taraba state.

2 Geologic setting

The study area is located in Ibi area of Taraba state which lies between latitude 8° 15′ N and 8° 30′ N and longitudes 9° 45′ E and 10° 00′ E. It is situated within the Middle Benue Trough, Nigeria, as shown in Fig. 1.

The Benue Trough is an intra-continental rift initiated in the Cretaceous during the opening of the South Atlantic Ocean. The formation of the trough has been associated with the opening of the southern Atlantic Ocean, and it is regarded as the failed arm or aulacogen of an RRR triple junction [14–16]. As a mainly structural basin of subsidence which was initiated as a product of basement disintegration, it was preceded by rifting during the Cretaceous continental split-up of South America and Africa plates [17, 18]. It is a major intra-continental sedimentary basin within the West to Central African region, spanning from Nigeria through Cameroon and eastwards to the Central African Republic. The width ranges between 150 and 250 km in Nigeria where it has been divided into three geological provinces (Fig. 2). Lithologically, these sub-basins are dominated by black carbonaceous shale in the Lower Benue, platform carbonates in the Middle Benue and sandstones in the Upper Benue [16, 19–22]. The Middle Benue, where this research was conducted, is underlain by a sequence of sedimentary cover rocks of shale, limestone and siltstone units of the Asu River Group and the Eze-Aku Formations which lie unconformably on Pan-African porphyritic granites (Fig. 3).

2.1 Structures and mineralization

The Albian to Coniacian sediments in the study area have been affected by the Santonian tectonic events which transformed the basin into anticlinal and synclinal landform with series of folds and faults. These events were followed by mafic to intermediate volcanic activities which emplaced volcanic rocks such as sills and dykes within the sediments [16, 27–29]. Lead–zinc–barytes mineralization occurs as lodes and veins in faults within the Albian–Cenomanian sediments of Asu River Group, Awe,

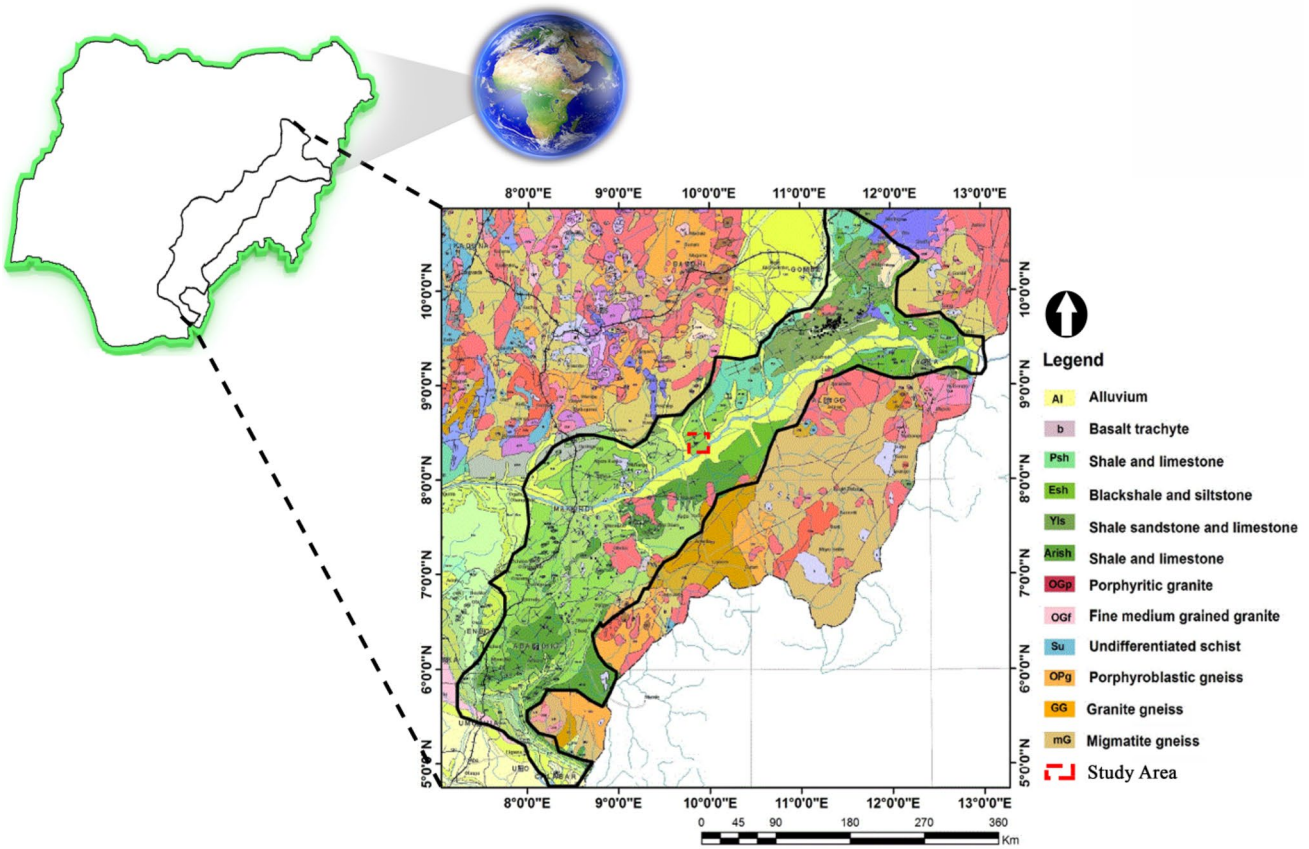

Fig. 1 Sectional geologic map of Nigeria showing the entire Benue Trough (modified after NGSA [13])

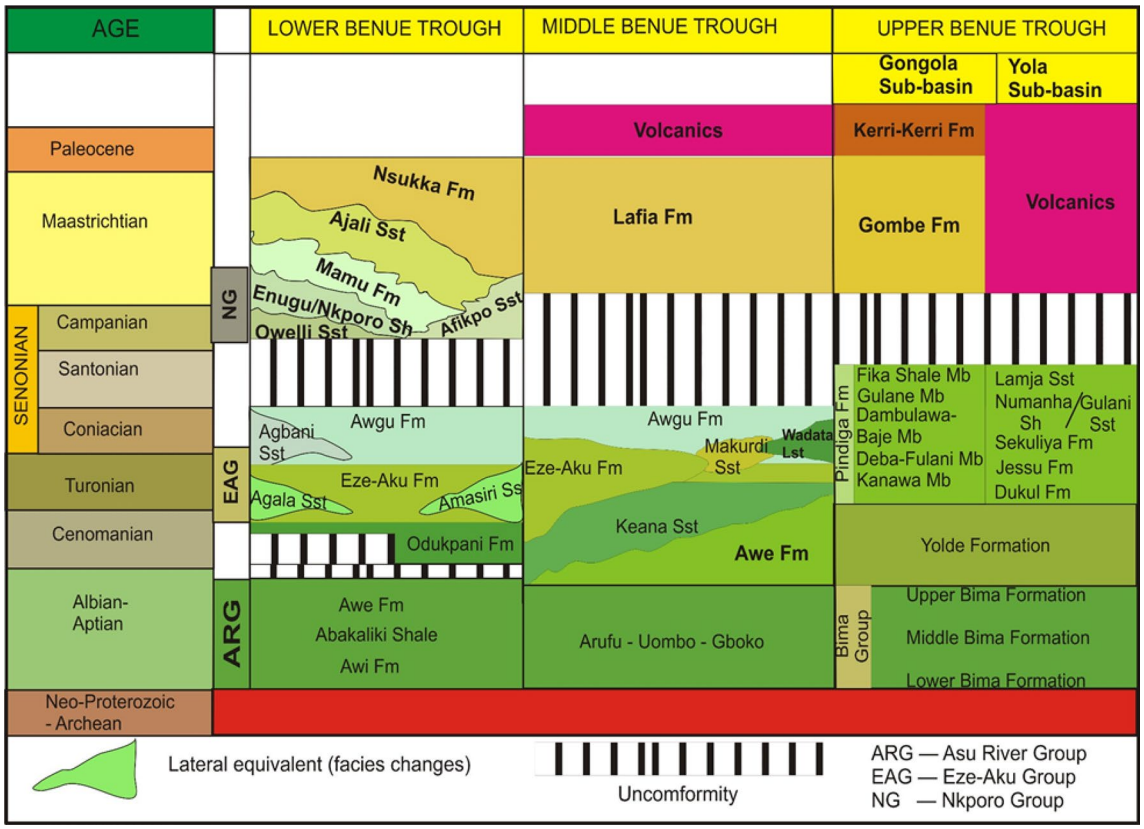

Fig. 2 Stratigraphy of the entire Benue Trough of Nigeria (modified after Carter et al. [22], Reyment [23], Offodile [24], Guiraud [25] and Zarborski [26])

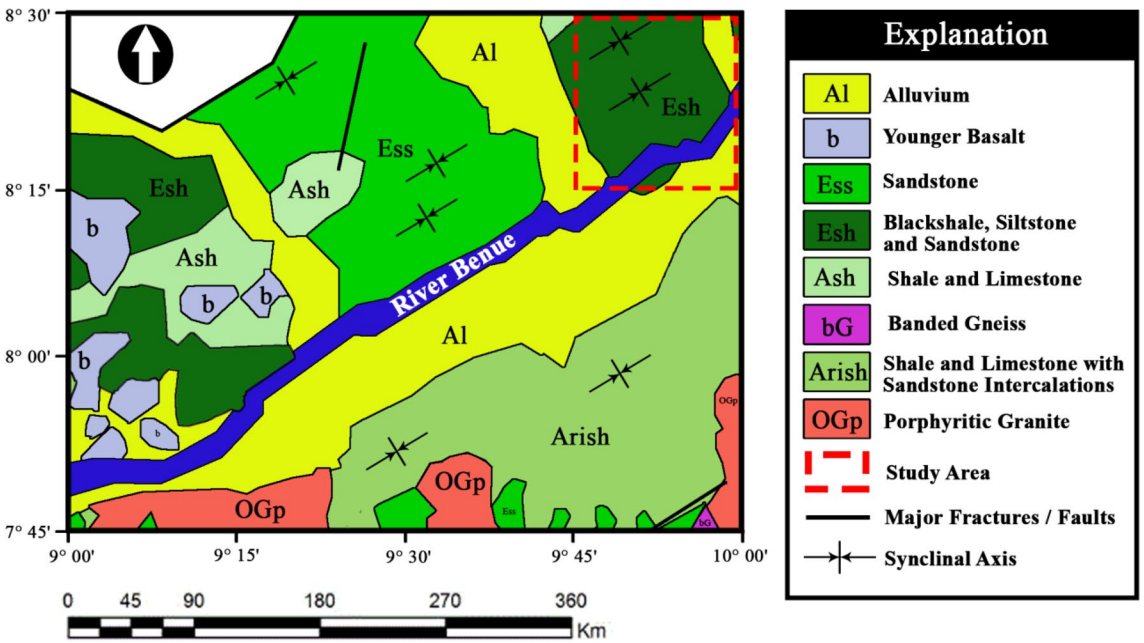

Fig. 3 Geological map of the Middle Benue Trough showing the study area indicated as red dashed lines (modified after NGSA [13])

Keana and Eze-Aku Formations. The fault patterns occur as linear structures or as different irregular faults that are interconnected and spaced over a considerable width and distance. The area of study in this paper around Wukari and Ibi is part of the known mineralized zones in the Middle Benue Trough [30]. Specifically, the area is located within the Wukari sub-basin [16] underlain by the Eze-Aku Formation which consists of hard gray and black cancerous shale, limestone and siltstone. This is overlain by bluish-gray bedded shale with fine-grained carbonaceous limestone bed of the Awgu Formation. These sediments along with the underlying older Albian Keana Formation were deformed during the Santonian episode that formed the Keana anticline. The study area lies within the adjoining synclinal axis generally referred to as the Giza syncline.

3 Data and methods

3.1 Data

The total magnetic intensity (TMI) anomaly data covering parts of Ibi area of Taraba state, Middle Benue Trough Nigeria, were provided by the Nigerian Geological Survey Agency (NGSA). The aeromagnetic survey was carried out by Fugro Airborne Surveys Limited for NGSA between 2004 and 2009, using 3 × Scintrex CS3 Cesium Vapor magnetometer along a series of NW–SE flight lines with a spacing interval of 500 m and sensor mean terrain clearance of 80 m while tie lines occur at about 2-km interval. A typical initial correction such as diurnal correction was applied to the aeromagnetic data and then gridded using minimum curvature technique with a grid cell of 100 m to produce the TMI data of the study area. The TMI is the vector sum of the two horizontal and the vertical components of the magnetic field [31]. TMI differs within various locations due to the strength and inclination of the Earth's magnetic field. The International Geomagnetic Reference Field (IGRF) correction was applied to the TMI data to remove the regional effect of the geomagnetic field. The resulting diurnal and IGRF-corrected TMI aeromagnetic anomaly map is shown in Fig. 4. At low-latitude regions such as the study area, magnetic geologic sources would be characterized normally by low magnetic anomalies.

3.2 Methods

The TMI aeromagnetic anomaly map was enhanced to estimate depth to magnetic basement and geometry of structural features (such as faults, fractures and dykes) within the study area. Standard enhancement techniques utilized include the upward continuation and

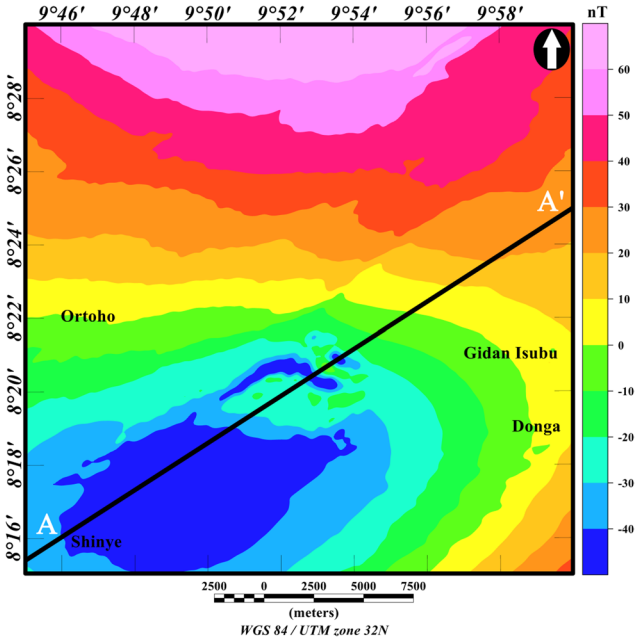

Fig. 4 Total magnetic intensity anomaly map of the study area. The 2D model for profile A–A′ is shown in Fig. 10

3D analytic signal methods as well as 3D Euler deconvolution to obtain locations and depths of structural features. Furthermore, the source parameter imaging (SPI) technique was used to estimate depth to magnetic basement. All analyses were performed using commercial software package Oasis Montaj (Geosoft™). The applied techniques have different advantages in various geologic situations. Utilizing multiple standard techniques to the same anomaly region improved the reliability of the deduced results. Since the analysis of observed anomalies is usually complicated by the lateral displacement of the magnetic anomalies with regard to their magnetic sources at nonpolar and non-equatorial latitudes, we first apply the reduction-to-pole (RTP) filter to the TMI anomaly map, assuming the magnetization of the sources is induced. Magnetic field intensity, inclination and declination are the parameters used for the application of the RTP filter. We select these parameter values at the midpoint of the study area (longitude 9° 52′ and latitude 8° 22′): total magnetic field value of 33,516 nT, inclination of − 7.564° and declination of − 1.471°. Also, we used amplitude correction inclination of − 90° to stabilize the result of the RTP transformation, which is not stable for low-latitude regions. After applying the RTP filter, the anomalies on the resulting RTP aeromagnetic anomaly map (Fig. 5) are shifted such that they are repositioned directly over their respective magnetic sources.

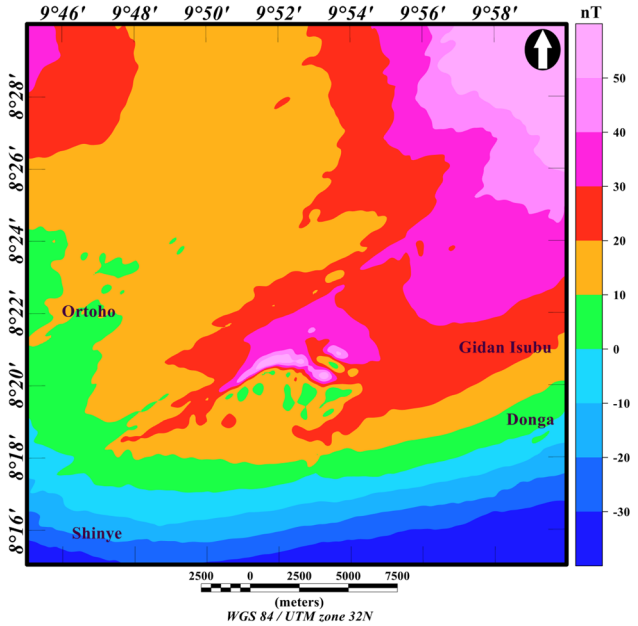

Fig. 5 Reduced-to-pole aeromagnetic anomaly map of the study area

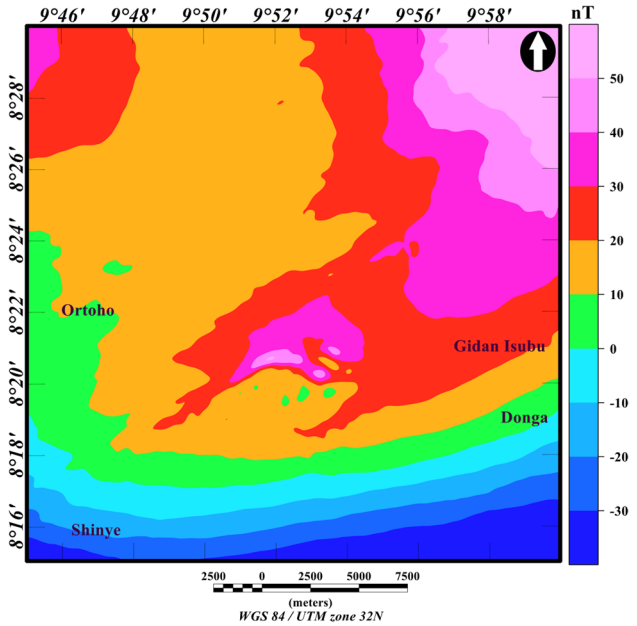

Fig. 6 Reduced-to-pole regional aeromagnetic anomaly map upward continued to a total elevation of 180 m

3.2.1 Upward continuation and subtraction from RTP anomaly data

Upward continuation of aeromagnetic anomaly data is commonly used by geophysicist to enhance the signal of deep and extended sources [32–34]. The upward continuation filter is considered a clean filter because it produces almost no side effects that may require the application of other filters or processes to correct. We applied the upward continuation filter (using 100 m increment) to the reduced-to-pole anomaly data (initially at 80 m above the ground) to produce a regional magnetic anomaly field, which would be measured on another surface with a total elevation of 180 m. The resulting regional magnetic field grid (see Fig. 6) was subsequently subtracted from the RTP aeromagnetic anomaly grid to produce a residual magnetic anomaly map (see Fig. 7a). Most anomalies that are shown in the RTP anomaly map (see Fig. 5) continues to the regional aeromagnetic map (Fig. 6).

3.2.2 3D analytic signal

Structural filters are crucial tools for outlining the edges, and hence the horizontal extent of magnetic sources and in Ibi area, these could be potential locations for mineral exploration targets [35]. The edges of magnetic sources within Ibi area can be examined by applying the 3D analytic signal (AS) filter. The major advantage of the 3D AS technique initially established for profile magnetic data by Nabighian [36] is that the 3D AS produces maxima over linear structural features (such as fractures, faults or dykes) and is independent of Earth's magnetic field parameters and the direction of magnetization of the magnetic bodies [9]. Therefore, the 3D AS algorithm does not require that the aeromagnetic anomaly data undergo either a reduction-to-pole or equator transformation. Roset et al. [9] showed that the absolute value (amplitude) of the 3D AS can be derived from the square root of the sum of the vertical and horizontal derivatives of the total magnetic field, using the relation:

$$|A(x,y)| = \sqrt{\left(\frac{\partial T}{\partial x}\right)^2 + \left(\frac{\partial T}{\partial y}\right)^2 + \left(\frac{\partial T}{\partial z}\right)^2} \quad (3)$$

where $\frac{\partial T}{\partial x}$, $\frac{\partial T}{\partial y}$, $\frac{\partial T}{\partial z}$ are the first derivatives of the total magnetic anomaly field.

The 3D AS filter was applied to the aeromagnetic anomaly data of Ibi area, in an attempt to map structural features within the study area.

3.2.3 3D Euler deconvolution

The 3D Euler deconvolution has proven to be a robust interpretation tool in magnetic data interpretation, because it requires little previous information about the geometry of the magnetic sources. Another advantage of this technique is that it requires no knowledge regarding the magnetization vector [10, 11]. Hence, it can be applied on regions where causative magnetic sources

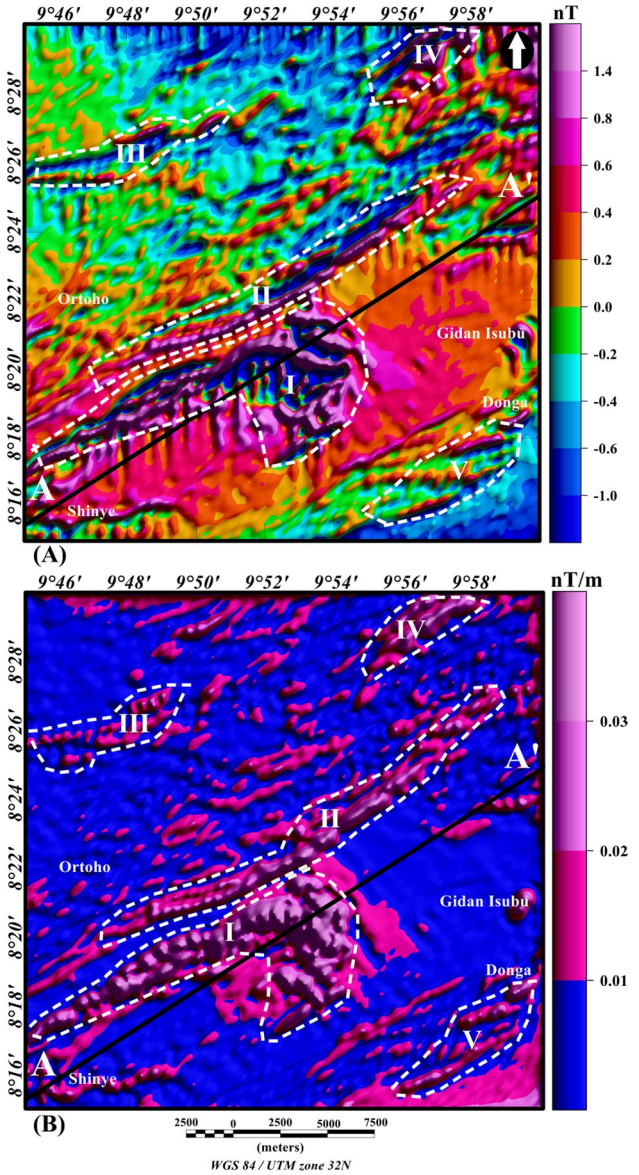

Fig. 7 Combined interpretation of structural features within the study area: **a** color-shaded reduced-to-pole residual magnetic anomaly map and **b** color-shaded 3D analytic signal map of the study area

are hidden and where geology of the location is poorly known. Largely, the technique has been used extensively to outline the edges and shapes of sources from potential field image [37]. The 3D Euler deconvolution equation is given as [11]:

$$(x-x_0)\frac{\partial T}{\partial x}+(y-y_0)\frac{\partial T}{\partial y}+(z-z_0)\frac{\partial T}{\partial z}=N(B-T) \quad (4)$$

where B is the regional value of the total magnetic field and (x_0, y_0 and z_0) are the coordinates of the magnetic source, which produces the total magnetic field T measured at x, y and z.

Table 1 3D Euler deconvolution magnetic structural indices [38]

S/N	Source type	SI
1	Contact of extensive depth extent	0
2	Edge thin sheet, sill, dike	1
3	Line, thin bed fault, cylinder	2
4	Sphere or compact body at a distance	3

N is identified as the structural index (SI); the values of SI for valid sources are given in Table 1. It is a measure of the decaying rate of the magnetic field with distance from the source. It gives a way to differentiate between various source shapes by signifying the magnetic anomaly attenuation rate at the observation point and relies on the source geometry [10]. In practice, the method is very suitable in characterizing dykes, sills, lineaments or other sharp lateral changes in magnetization [38]. The aeromagnetic anomaly data were subjected to 3D Euler deconvolution analysis in order to map structural features within the study area. The aeromagnetic anomaly data were subjected to 3D Euler deconvolution analysis in order to calculate depth values of subsurface structural features within the study area.

3.2.4 Source parameter imaging

The analysis and interpretation of a magnetic anomaly response involves estimating the parameters that characterize the source of the magnetic anomaly. Hence, we utilized the source parameter imaging (SPI) technique to estimate the depths to top of magnetic sources [12]. The technique does not require assumption of structural index to estimate depth of sources [39]. The SPI uses the local wavenumber, denoted $K(x,y)$, which is given by the expression:

$$K(x,y)=\frac{\frac{\partial^2 T}{\partial x\partial z}\frac{\partial T}{\partial x}+\frac{\partial^2 T}{\partial x\partial z}\frac{\partial T}{\partial y}+\frac{\partial^2 T}{\partial z^2}\frac{\partial T}{\partial z}}{|A(x,y)|^2} \quad (5)$$

where $|A(x,y)|$ is given by Eq. 3. For a dipping magnetic contact, peaks of $K(x,y)$ are positioned directly over the edges of the isolated geologic contacts and are independent of magnetic declination, inclination, strike and dip [40]. Hence, it is not required to reduce the aeromagnetic anomaly data to the magnetic pole/equator. Consequently, the estimations of depth to magnetic sources are obtained from the reciprocal of the local wavenumber as:

$$Depth_{x=0}=\frac{1}{K(x,y)_{\max}} \quad (6)$$

where the maximum value of local wavenumber $K(x, y)$ over the step magnetic source is given as $K(x, y)_{max}$. Additionally, the SPI technique has two major advantages: It does not depend on selected window size, and it eliminates errors initiated by survey lines [12, 40]. Therefore, we used the SPI to estimate the depths to magnetic basement of the studied region.

4 Results and interpretation

The visual inspection of the regional aeromagnetic anomaly map shows good correlation with the reduced-to-pole (RTP) anomaly map in terms of trends and patterns of anomalies. This similarity shows that majority of the causative sources within the studied region are of deeper origin. The RTP and regional aeromagnetic maps reveal circular, semicircular to elongated anomalies with E–W, NW–SE and NE–SW trends. These maps show high- and low-amplitude anomalies between − 30 and 50 nT. The high-amplitude anomalies which are located at the central and northeastern parts of the study area are attributed to intrusive bodies and/or uplifted basement blocks. The low-amplitude anomalies are probably due to low-frequency contributions associated with deeper crustal portion.

4.1 Structural features

The reduced-to-pole (RTP) residual magnetic anomaly map shown in Fig. 7a is typically a structural map [41], highlighting geologic features obscured by strong regional magnetic effect. The RTP residual magnetic anomaly map depicts effects of near-surface structural features but cannot provide information for deep-seated features. In order to overcome this problem, we used the 3D AS map (Fig. 7b) to complement the RTP residual map (Fig. 7a). Visual integration of the RTP residual and 3D AS maps facilitated the division of the study area into five structural zones which provide vital information regarding regional structural features such as faults, folds and intrusions.

4.1.1 Zone I

This domain is located at the northern edge of the River Benue and extends from the southwestern part of the study area to the central part, with a parallel alignment to the River Benue. There are three structural trends within this domain as shown in Fig. 7a, b: the broad NE–SW-trending structural features which are the dominant trends and the minor N–S and NW–SE trends which occur as associated structures to the former. This domain is suspected to be associated with vein barite mineralization [42]. The minor N–S and NW–SE trends are more visible on the 3D analytic signal map shown in Fig. 7b; this pattern has been documented to be associated with barites mineralization [42, 43]. The NE-trending structural features are almost elliptical in shape, and its magnitude is higher than the associated structural features. As a result of the pattern of formation and the magnitude of the structures, we tentatively interpret the trend pattern as evidence of minor folds that form part of the main asymmetrical synclinorium—Giza synclinorium.

4.1.2 Zone II

The anomaly with elongation along NE-SW trend within the zone originated from southwestern part of the study area extends to the northeastern part (Fig. 7). Due to the pattern and extent covered by this anomaly, we tentatively interpret the anomaly as a major fault zone within the Giza syncline associated with lead–zinc mineralization. The fault is parallel to the axis of the interpreted folds in zone I and is therefore regarded to be a strike-slip fault. The interpreted fault may in fact be attributed to the Giza fault suggested by Ajayi and Ajakaiye [43] around the study area. Additionally, the occurrence of this anomaly is consistent with vein structures which stretch for 5 to 6 km at Bukuyu village in Ibi [42, 44].

4.1.3 Zone III

This zone is more clearly revealed on the residual anomaly map (Fig. 7a) in comparison with the 3D analytic signal map (Fig. 7b). The anomaly within this zone is thin, short with ENE trend and located entirely at the northeastern part of the study area. We interpret this anomaly as an intrusive structural feature in the form of sill (probably dolerite). Our interpretation is consistent with the report of Ofoegbu [45] around the study area, and the researcher revealed the occurrences of intrusive structures in the form of sills (probably dolerite) within the Middle Benue Trough with ENE trends.

4.1.4 Zone IV

This zone is clearly revealed on both the residual magnetic anomaly map (Fig. 7a) and 3D analytic signal map (Fig. 7b). It is located entirely at the northeastern part of the region under study. The anomaly within this zone trend NE–SW with the linear to curvilinear pattern extends beyond the study area at the NE edge of the maps (Fig. 7a, b). Based on the trend and pattern of the anomaly, we interpret the anomaly as a fold which forms a minor syncline within the bigger Giza synclinorium. The anomaly shows similar pattern with the interpreted folds in zone I, although its full extent is not shown in Fig. 7.

4.1.5 Zone V

The anomalies within this zone are clearly revealed as a linear pattern on the residual magnetic map (Fig. 7a), but more clearly shown and well distinct on the 3D analytic signal map (Fig. 7b). This zone is situated entirely within the southeastern part of the study area. The anomalies within this zone are thin and trend E–W and NE–SW. As a result of the pattern of formation and magnitude of the anomalies, we interpret these anomalies as buried volcanic intrusions such as dykes and sills within the sedimentary formations. Such intrusions have been confirmed and established by drilling to exist around the region [43]. Also, Chukwu [46, 47] confirmed the existence of such volcanic intrusions through field geologic mapping around the area, while Oden [42] suggested sediment-hosted barite occurrences of hydrothermal origin in Gidanwaya of Ibi area.

4.1.6 Depth estimates of structural features

We applied the 3D Euler deconvolution technique to aeromagnetic anomaly data to estimate possible depths of the mapped structural features shown in the 3D analytic signal and residual anomaly maps (see Fig. 7). The structural indices (SI) shown in Table 1 generate better clustering solutions for different geologic source types, as should be expected. We choose SI of 0 and 1 because of the available geological information of the region under study, and they are the best-fit indices based on the scope of this study. The following conditions were used to actualize the 3D Euler depth solution maps of Ibi area.

- The locations and depth estimations of intrusive structural features such as dykes, sills and veins are realized using SI of 1.0, depth tolerance error of 12% and window size of 2000 m square grids.
- The estimation of depths and locations of geological contacts was achieved, using window size of 2000 m, SI of 0.0 and maximum depth tolerance of 10%.

Utilizing these relations, we produced the 3D Euler depth solution maps of Ibi area shown in Fig. 8a, b. The maps depict clearly locations, trends and depth information of different structural features within the study area. The interesting observations on the maps are the trends and locations of structural features which correlate perfectly with those depicted on the residual magnetic map (Fig. 7a) and 3D analytic signal map (Fig. 7b). Furthermore, the 3D Euler depth solution maps revealed solutions for depth values between 200 m and 600 m within the study area. The first obvious pattern on the 3D Euler depth solution map for SI = 1.0 (Fig. 8b) is the interpreted zone I on the residual magnetic map (Fig. 7a) and 3D analytic signal map (Fig. 7b). Also, the 3D Euler depth solution map SI = 1.0 (Fig. 8b) confirms the interpreted structural features within zones II, III and IV on the residual magnetic map (Fig. 7a) and analytic signal map (Fig. 7b). The southeastern part of the 3D Euler depth solution map for SI = 0.0 is marked by a major alignment with NE–SW trend which correlates perfectly with similar pattern and trend observed on the SE part of residual magnetic map (Fig. 7a) and 3D analytic signed map (Fig. 7b).

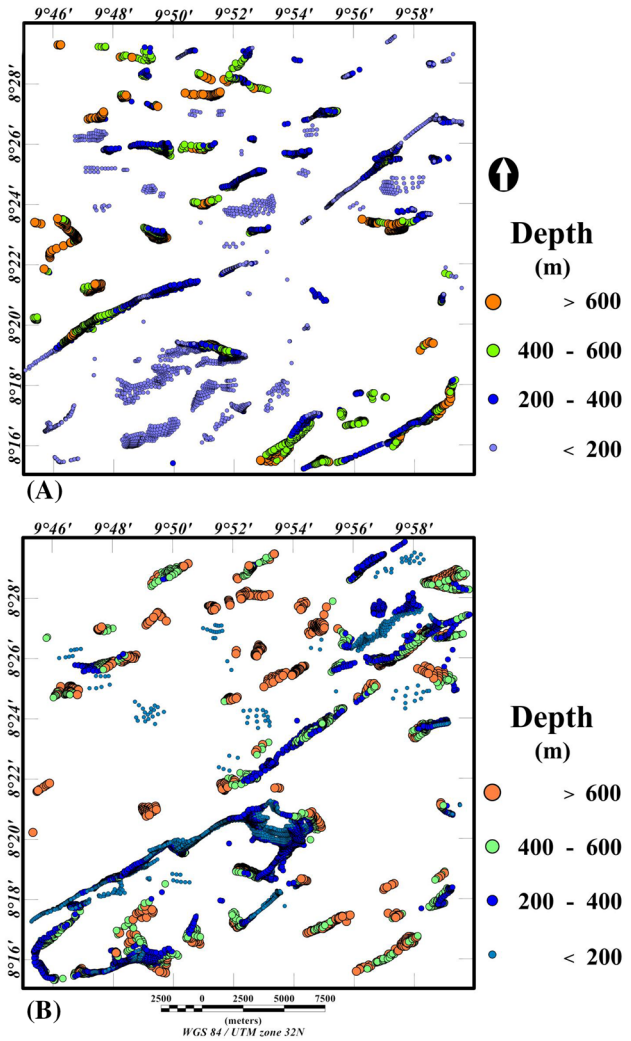

Fig. 8 3D Euler deconvolution maps for structural index (SI) of 0 and 1, produced from the aeromagnetic anomaly data of the study area: **a** 3D Euler solution map for SI = 0.0 and **b** 3D Euler solution map for SI = 1.0

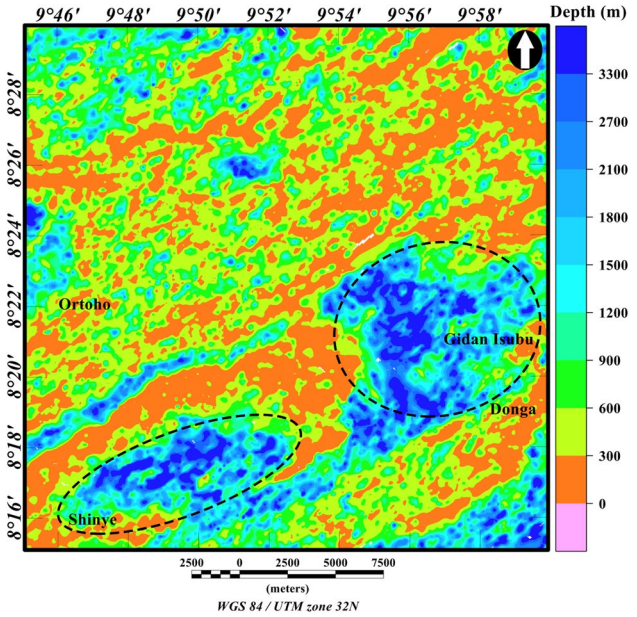

Fig. 9 Magnetic basement depth map estimated utilizing source parameter imaging method. The dashed black lines indicate two deep zones which are probably the hydrocarbon provinces of the study area

4.2 Magnetic basement depth estimates

4.2.1 Source parameter imaging

The source parameter imaging (SPI) technique was used for automatic estimate of magnetic source depths from the aeromagnetic anomaly data, which could provide significant information regarding the hydrocarbon potential of the region. Previous assessment of the hydrocarbon potential of succession in the Benue Trough showed a number of rich organic intervals capable of yielding large quantities of hydrocarbon within the Cretaceous section [48]. The resulting SPI map is presented in Fig. 9, indicating spatial locations of numerous magnetic sources at various depths within the study area. The map shows two deep zones characterized by blue color with depths values between 2700 and 3300 m which are suspected to be the hydrocarbon provinces of the study area, because of substantial sedimentary thickness, in addition to the mapped structural features and established stratigraphic information of the region. We interpret these deep zones as the locations of the depocenters within the study area, which are indicated as dashed black lines. These zones are

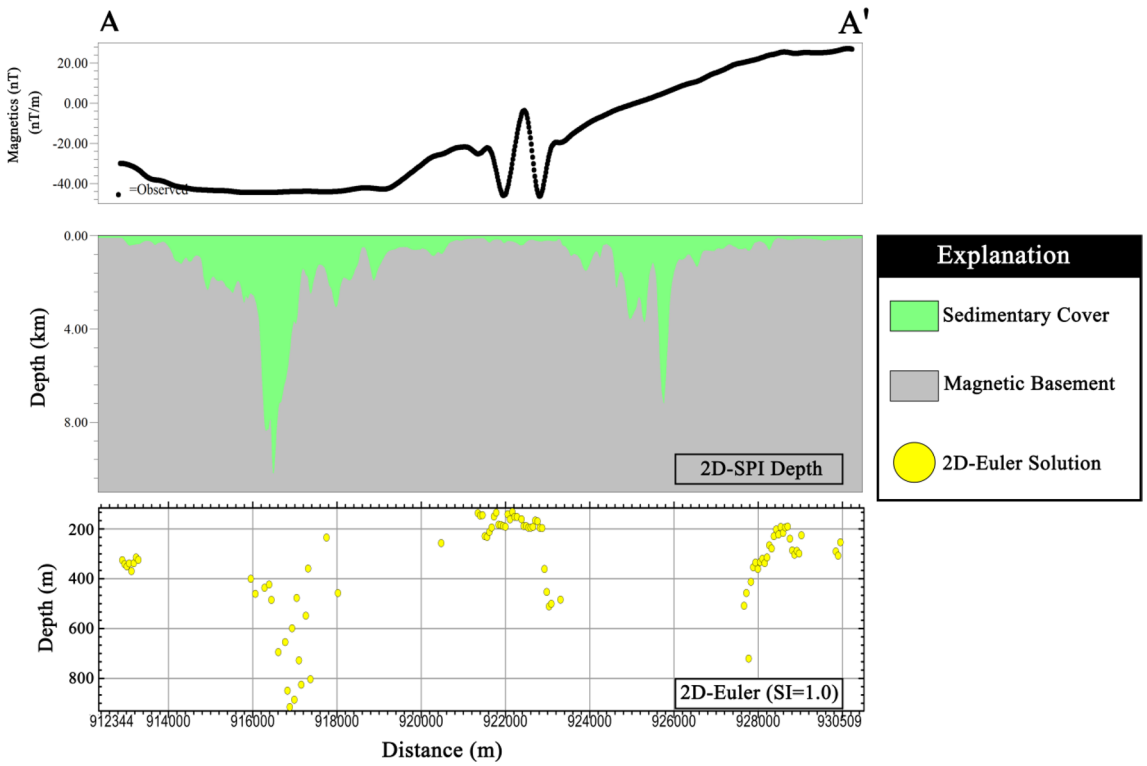

Fig. 10 2D Euler and 2D SPI depth model for profile A–A′, across zone I (located in Fig. 7). The observed magnetic curve was extracted from the aeromagnetic anomaly grid (Fig. 4)

surrounded by folds and numerous intrusive bodies which are capable of providing the required minimum temperature for hydrocarbon maturation in addition to their trapping qualities. Wright et al. [49] described that the lowest sedimentary thickness essential to realize the threshold temperature of 115 °C for the initiation of hydrocarbon would be 2300 m thick when all other conditions for fossil maturation are favorable. The indicated deep zones on the SPI map have shown good potential hydrocarbon provinces within the study area, which shares obvious and common stratigraphic continuity with the Gongola Basin where three exploratory wells have been drilled: Kuzari-1, Nasara-1 and Kolmani River-1 [48]. The interpreted folds in zone I in Fig. 6 are also visible on the SPI map which can act as hydrocarbon traps. The interpreted model shown in Fig. 9 runs approximately from southwestern to eastern part of the study area which traverses the interpreted depocenter on the SPI map, in addition to the anomalies in zone I on the residual anomaly map (Fig. 7a) and 3D analytic signal map (Fig. 7b). The 2D Euler deconvolution contributed to obtaining the depth values of suspected edges of folds interpreted in zone I is shown in Fig. 7. This technique, coupled with the 2D SPI depth model, revealed high hydrocarbon potential of adequate sedimentary pile within the delineated deep zones (shown in Fig. 9). This is corroborated by the recent discovery of hydrocarbon in Kolmani River-II within Gongola Basin-Upper Benue Trough [50], which shares common stratigraphic characteristics with Ibi area. Additionally, the depth values of the structural features on the SPI map show compelling alignment of results with the structural features shown in the 3D Euler depth solution map for structural index 1.0 (Fig. 8b).

5 Conclusion

The analysis and interpretation of high-resolution aeromagnetic anomaly data of Ibi area allows the delineation of locations, trends and extent of regional structural features, in addition to detailed depth information regarding the underneath basement. The interpretation of the residual magnetic and 3D analytic signal maps reveals five structural zones within the study area (Fig. 7). The interpreted structural features within these zones are linear to curvilinear with N–S, NE–SW, NW–SE and ENE–WSW trends. The structural features represent faults, folds and intrusions. The 3D Euler deconvolution depth maps provide additional information regarding various aspects of these structural features, such as the size, depth, extension and trends. Also, the source parameter imaging map indicates the depths to magnetic basement of the region which ranges from 0 to 3300 m with an average depth value of 1650 m. This map shows two deep zones with estimated depth values between 2700 m and 3300 m which are likely to be the hydrocarbon provinces of the study area. Additionally, the shallow depth values on the source parameter imaging map show compelling alignment of depth results with structure features shown in the 3D Euler depth solution map for structural index 1.0. These results reveal information of subsurface configuration of the study area which is essential for hydrocarbon and mineral exploration projects within the region.

Acknowledgements The authors would like to thank BS Geophysical and Consultancy Ltd., for their support and the facilities made available during the course of this work.

Compliance with ethical standards

Conflict of interest The authors declare that they have no conflict of interest.

References

1. Supper R, Baron I, Ottowitz D, Motschka K, Gruber S, Winkler E, Jochum B, Römer A (2013) Airborne geophysical mapping as an innovative methodology for landslide investigation: evaluation of results from the Gschliefgraben landslide, Austria. Nat Hazards Earth Sys Sci 13:3313–3328
2. Waswa AK, Nyamai CM, Mathu E, Ichang'i DW (2015) Application of magnetic survey in the investigation of iron ore deposits and shear zone delineation: case study of Mutomo-Ikutha area, SE Kenya. Int J Geosci 6:729
3. Sundararajan N, Pracejus B, Al-Khirbash S, Al-Hosni T, Ebrahimi A, Al- Mushani M (2017) Magnetic mapping for delineating structures favorable to uranium mineralization in Dhofar region, Sultanate of Oman. Int J Earth Environ Sci 1:127
4. Nabighian MN, Grauch VJS, Hansen RO, LaFehr TR, Li Y, Peirce JW, Phillips JD, Ruder ME (2005) The historical development of the magnetic method in exploration. Geophysics 70:33–61
5. Gunn P (1997) Airborne magnetic and radiometric survey. J Aust Geol Geophys 2:216
6. Reeves CV, Reford SW, Milligan PR (1997) Airborne geophysics: old methods, new images. In: Gubbins AG (ed) Proceedings of exploration 97, fourth decennial international conference on mineral exploration, pp 13–30
7. Reeves CV (1998) Continental scale and global geophysical anomaly mapping. ITC J 2:91–98
8. Nabighian MN (1984) Toward a three-dimensional automatic interpretation of potential field data via generalized Hilbert transforms: fundamental relations. Geophysics 49:780–786
9. Roest WR, Verhoef J, Pilkington M (1992) Magnetic interpretation using the 3-D analytic signal. Geophysics 57:116–125
10. Thompson DT (1982) EULDPH: a new technique for making computer-assisted depth estimates from magnetic data. Geophysics 47:31–37
11. Reid AB, Allsop JM, Granser H, Millett AJ, Somerton IW (1990) Magnetic interpretation in three dimensions using Euler deconvolution. Geophysics 55:80–91

12. Thurston JB, Smith RS (1997) Automatic conversion of magnetic data to depth, dip, and susceptibility contrast using the SPI (TM) method. Geophysics 62:807–813. https://doi.org/10.1190/1.1444190
13. Nigerian Geological Survey Organization (NGSA) (2006) Mineral resources map of Nigeria, 1 map scale 1:2,000,000
14. Burke KC, Dessauvagie TFJ, Whiteman AJ (1972) Geological history of the Benue Valley and adjacent areas. In: Dessauvagie TFJ, Whiteman AJ (eds) African geology. Ibadan University Press, Ibadan, pp 187–205
15. Olade MA (1975) Evolution of Nigeria's Benue Trough (Aulacogen): a tectonic model. Geol Mag 112(06):575. https://doi.org/10.1017/s001675680003898x
16. Benkhelil J (1989) The origin and evolution of the Cretaceous Benue Trough (Nigeria). J Afr Earth Sc 8:251–282
17. Grant NK (1971) The South Atlantic Benue Trough and Gulf of Guinea Cretaceous triple Junction. Geol Soc Am Bull 82:2295–2298
18. Akande SO, Mucke A (1989) Mineralogical, textural and paragenetic studies of the lead–zinc–copper mineralization in the lower Benue Trough (Nigeria) and their genetic implications. J Afr Earth Sc 9:23–29
19. Maurin JC, Benkhelil J, Robineau B (1986) Fault rocks of the Kaltungo lineament (NE Nigeria) and their relation with Benue Trough tectonic. J Geol Soc 143:587–599
20. Rebelle M (1990) The marine transgression in the Benue Trough (N.E Nigeria) a paleogeographic interpretation of the Gongila Formation. J Afr Earth Sc 10:643–656
21. Oha IA, Onuoha KM, Dada SS (2017) Contrasting styles of lead–zinc–barium mineralization in the Lower Benue Trough, Southern Nigeria. Earth Sci Res J 21:7–16
22. Carter JD, Barber W, Tait EA (1963) Geology of parts of Adamawa, Bauchi and Bornu provinces in Northeastern Nigeria. Bull Geol Surv Niger 30:1–108
23. Reyment RA (1965) Aspects of the geology of Nigeria. Ibadan University Press, Ibadan
24. Offodile ME (1976) A review of the geology of the Cretaceous of the Benue Trough. In: Kogbe CA (ed) Geology of Nigeria. Elizabethan Publishing Co., Lagos, pp 319–330
25. Guiraud M (1989) Tectono-sedimentary framework of the Early Cretaceous continental Bima Formation (Upper Benue Trough, NE Nigeria). J Afr Earth Sci Spec Publ 10:341–353
26. Zaborski PM (1998) A review of the Cretaceous System in Nigeria. Afr Geosci Rev 5:385–483
27. Short KC, Stauble AJ (1967) Outline of geology of Niger Delta. Am Assoc Petrol Geol Bull 51:761–779
28. Murat RC (1972) Stratigraphy and paleogeography of the Cretaceous and Lower tertiary in southern Nigeria. In: Dessauvagie TFJ, Whiteman AJ (eds) African Geology. University Press, Ibadan
29. Samaila NK, Likkason OK (2013) Role of equatorial fracture zones on fluid migration across the south Atlantic margins. J Earth Sci Clim Change. https://doi.org/10.4172/2157-7617.S12-004
30. Fatoye FB, Ibitomi MA, Omada JI (2014) Lead–zinc–barytes mineralization in the Benue Trough, Nigeria: their geology, occurrences and economic prospective. Adv Appl Sci Res 5:86–92
31. Dentith M, Mudge ST (2014) Geophysics for the mineral exploration geoscientist. Cambridge University Press, Cambridge
32. Fedi M, Rapolla A, Russo G (1999) Upward continuation of scattered potential field data. Geophysics 64(2):443–451
33. Robinson E (1970) Upward continuation of total intensity magnetic fields. Geophysics 35(5):920–926
34. Ciminale M, Loddo M (1989) A computer program to perform the upward continuation of potential field data between arbitrary surfaces. Comput Geosci 15(6):889–903. https://doi.org/10.1016/0098-3004(89)90003-4
35. Salawu NB, Olatunji S, Adebiyi LS, Olasunkanmi NK, Dada SS (2019) Edge detection and magnetic basement depth of Danko area, northwestern Nigeria, from low- latitude aeromagnetic anomaly data. SN Appl Sci 1:1056. https://doi.org/10.1007/s42452-019-1090-3
36. Nabighian MN (1972) The analytic signal of two-dimensional magnetic bodies with polygonal cross-section; its properties and use for automated anomaly interpretation. Geophysics 37:507–517
37. Salawu NB, Olatunji S, Orosun MM, Abdulraheem TY (2019) Geophysical inversion of geologic structures of Oyo Metropolis, Southwestern Nigeria from airborne magnetic data. Geomech Geophys Geo-energy Geo-Resour 5:143–157
38. Reid AB, Ebbing J, Webb SJ (2013) Avoidable Euler errors—the use and abuse of Euler deconvolution applied to potential fields. Geophys Prospect. https://doi.org/10.1111/1365-2478.12119
39. Phillips JD, Hansen OR, Blakely RJ (2007) The use of curvature in potential-field interpretation. Explor Geophys 38:111–119
40. Agustina P, Mario EG, Guido MG, Andrés F, Patricia M (2018) Magnetic characterization of a retroarc extensional basin: the Loncopué Trough. J S Am Earth Sci 89:55–62
41. Finn CA, Horton JD (2015) Crystalline basement map of Mauritania derived from filtered aeromagnetic data (phase V, deliverable 54_1), aeromagnetic and geological structure map of Mauritania (phase V, deliverable 54_2), maximum depth to basement map of Mauritania derived from Euler analysis of aeromagnetic data (phase V, deliverable 54_3), and color composite image of radioelement data (added value), chap. B1. In: Taylor CD (ed) Second projet de renforcement institutionnel du secteur minier de la République Islamique de Mauritanie (PRISM-II): U.S. Geological Survey Open-File Report 2013—1280-B1, 4 pl., scale 1:1,000,000, http://dx.doi.org/10.3133/ofr20131280/
42. Oden MI (2012) Barite veins in the Benue Trough: field characteristics, the quality issue and some tectonic implications. Environ Nat Resour Res 2(2):21–31
43. Ajayi CO, Ajakaiye DE (1986) Structures deduced from gravity data in the Middle Benue, Nigeria. J Afr Earth Sci 5(4):359–369
44. Edu EE (2006) Interim report on assessment of barite resources in Taraba State, Nigeria. N.G.S.A Report (unpublished)
45. Ofoegbu CO (1985) A review of the geology of the Benue Trough, Nigeria. J Afr Earth Sci 3(3):283–291
46. Chukwu DU (1983) Lower Cretaceous alkaline rhyolite sills along curved fractures in sedimentary graben-like depression around Tseagu-Tseagodo Hills, SE Middle Benue Margin, Nigeria. In: International conference on alkaline ring complexes in Africa (Zaria and Jos, December 1983), abstracts vol, p 30
47. Chukwu DU (1984) Early Cretaceous alkaline rhyolite sills along curved fractures around Tseagu-Tseagodo Hills, Southeastern Middle Benue Margin, Nigeria. In: 20th annual conference of Nigerian Mining and Geosciences Society, Nsukka, March 1984, abstract vol, p 18
48. Akande SO, Egenhoff SO, Obaje NG, Ojo OJ, Adekeye OA, Erdtmann BD (2012) Hydrocarbon potential of Cretaceous sediments in the Lower and Middle Benue Trough, Nigeria: insights from new source rock facies evaluation. J Afr Earth Sc 64:34–47
49. Wright JB, Hastings D, Jones WB, Williams HR (1985) Geology and mineral resources of West Africa. George Allen and Urwin, London, pp 90–120
50. NNPC (2019) A press release by the Corporation's Acting Group General Manager, Group Public Affairs Division. https://www.nnpcgroup.com/Pages/Home.aspx. Accessed 25 Oct 2019

Terms and Conditions

Springer Nature journal content, brought to you courtesy of Springer Nature Customer Service Center GmbH (“Springer Nature”).
Springer Nature supports a reasonable amount of sharing of research papers by authors, subscribers and authorised users (“Users”), for small-scale personal, non-commercial use provided that all copyright, trade and service marks and other proprietary notices are maintained. By accessing, sharing, receiving or otherwise using the Springer Nature journal content you agree to these terms of use (“Terms”). For these purposes, Springer Nature considers academic use (by researchers and students) to be non-commercial.
These Terms are supplementary and will apply in addition to any applicable website terms and conditions, a relevant site licence or a personal subscription. These Terms will prevail over any conflict or ambiguity with regards to the relevant terms, a site licence or a personal subscription (to the extent of the conflict or ambiguity only). For Creative Commons-licensed articles, the terms of the Creative Commons license used will apply.
We collect and use personal data to provide access to the Springer Nature journal content. We may also use these personal data internally within ResearchGate and Springer Nature and as agreed share it, in an anonymised way, for purposes of tracking, analysis and reporting. We will not otherwise disclose your personal data outside the ResearchGate or the Springer Nature group of companies unless we have your permission as detailed in the Privacy Policy.
While Users may use the Springer Nature journal content for small scale, personal non-commercial use, it is important to note that Users may not:

1. use such content for the purpose of providing other users with access on a regular or large scale basis or as a means to circumvent access control;
2. use such content where to do so would be considered a criminal or statutory offence in any jurisdiction, or gives rise to civil liability, or is otherwise unlawful;
3. falsely or misleadingly imply or suggest endorsement, approval , sponsorship, or association unless explicitly agreed to by Springer Nature in writing;
4. use bots or other automated methods to access the content or redirect messages
5. override any security feature or exclusionary protocol; or
6. share the content in order to create substitute for Springer Nature products or services or a systematic database of Springer Nature journal content.

In line with the restriction against commercial use, Springer Nature does not permit the creation of a product or service that creates revenue, royalties, rent or income from our content or its inclusion as part of a paid for service or for other commercial gain. Springer Nature journal content cannot be used for inter-library loans and librarians may not upload Springer Nature journal content on a large scale into their, or any other, institutional repository.
These terms of use are reviewed regularly and may be amended at any time. Springer Nature is not obligated to publish any information or content on this website and may remove it or features or functionality at our sole discretion, at any time with or without notice. Springer Nature may revoke this licence to you at any time and remove access to any copies of the Springer Nature journal content which have been saved.
To the fullest extent permitted by law, Springer Nature makes no warranties, representations or guarantees to Users, either express or implied with respect to the Springer nature journal content and all parties disclaim and waive any implied warranties or warranties imposed by law, including merchantability or fitness for any particular purpose.
Please note that these rights do not automatically extend to content, data or other material published by Springer Nature that may be licensed from third parties.
If you would like to use or distribute our Springer Nature journal content to a wider audience or on a regular basis or in any other manner not expressly permitted by these Terms, please contact Springer Nature at

onlineservice@springernature.com